Reactive nanojets: Nanostructure-enhanced chemical reactions in a defected energetic crystal

Ken-ichi Nomura, Rajiv K. Kalia, Aiichiro Nakano, and Priya Vashishta[a)]
Collaboratory for Advanced Computing and Simulations, Departments of Chemical Engineering & Materials Science, Physics & Astronomy, and Computer Science, University of Southern California, Los Angeles, California 90089-0242, USA

(Received 11 August 2007; accepted 11 October 2007; published online 2 November 2007)

Nanofluidics of chemically reactive species has enormous technological potential and computational challenge arising from coupling quantum-mechanical accuracy with largescale fluid phenomena. Here, we report a million-atom reactive force field molecular dynamics simulation of shock initiation of an energetic crystal with a nanometer-scale void. The simulation reveals the formation of a nanojet which focuses into a narrow beam at the void. This, combined with the excitation of vibrational modes through enhanced intermolecular collisions by the free volume of the void, catalyzes chemical reactions that do not occur otherwise. We also observe a pinning-depinning transition of the shock wave front at the void at increased particle velocity and the resulting localization-delocalization transition of the vibrational energy. © *2007 American Institute of Physics*. [DOI: 10.1063/1.2804557]

Recent advances in nanofluidics have shown unique fluid behavior in micro to nano meter scales, where properties of individual molecules become prominent rather than their averaged behavior.[1] One example is the enormous energy release from collapsing microbubbles.[2,3] A similar phenomenon is observed during shock compression of an energetic material[4–8] (EM) with a void.[2,9] Here, the formation of a nanojet at a void upon the arrival of a shock wave is expected to play an essential role in the reactivity of EMs. A long-standing problem in EMs is how nanostructures affect molecular decomposition processes under external stimuli. For example, energetic crystals with defects such as voids, grain boundaries, and cracks are known to be more sensitive to shock ignition than a perfect crystal. Defect sites in the crystal form higher-temperature regions, and mechanisms underlying these hotspot formation due to void collapse have attracted a great deal of attention and been extensively studied in recent years.[10–13]

Molecular dynamics (MD) simulations are ideally suited for the spatiotemporal regime of a nanojet. The challenge in simulating a reactive nanojet is to incorporate quantum mechanics into large scale MD simulation. Recent advances in semiempirical reactive force field[14,15] (REAXFF) and their scalable implementation on massively parallel computers have enabled the requisite coupling between quantum-mechanically accurate chemical reactions and large length-scale mechanical processes to study chemical reaction pathways under extreme conditions. To describe chemical bond breakage and formation, the REAXFF potentials are designed to include chemical bond orders and electronic charge transfer of all constituent atomic pairs by a charge equilibration[16,17] scheme. We have developed a fast reactive force field (F-REAXFF) algorithm to enable multimillion-atom REAXFF MD simulations on massively parallel computers.[18]

In this paper we report million-atom parallel F-REAXFF MD simulations of reactive nanofluidics in an energetic crystal under shock loading. We have performed planar shock simulations with two particle velocities V_p=1 and 3 km/s on a $C_3H_6O_6N_6$ (RDX) single crystal. A spherical void with an 8 nm diameter is introduced by removing molecules whose centers of mass are within 4 nm from the center of the system. The x, y, and z axes correspond to the [100], [010], and [001] crystallographic orientations, respectively. After introducing the void, the RDX system was relaxed for 3.5 ps at a temperature of 5 K. Subsequently, periodic boundary conditions were removed to create free surfaces in the y-z plane, and again the system was relaxed for 2 ps at 5 K. The dimensions of the total system including the vacuum layers are $358.50 \times 213.06 \times 203.82$ Å^3. A planar shock in the [100] direction is applied with a momentum mirror by reflecting the momentum of an atom whose position crosses the mirror plane. The RDX crystal is initially assigned a translational velocity $-V_p$ in the x direction toward the momentum mirror.

Figure 1 shows the velocity of RDX molecules. Here arrows at the molecular centers of mass are color coded by the magnitude of molecular velocities. For clarity, only a thin slice with 15 Å thickness is shown. A straight shock front

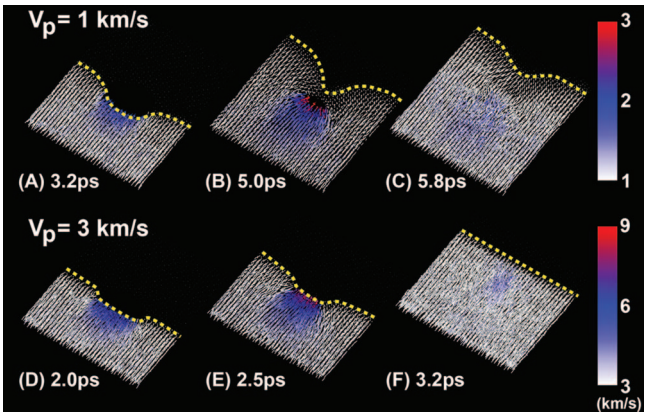

FIG. 1. (Color) Snapshots of velocity distribution of RDX molecules at V_p=1 km/s [(a)–(c)] and 3 km/s [(d)–(f)]. Arrows are color coded by the magnitude of velocity. At V_p=1 km/s, the shock front is pinned at the void and bends (3.2–5 ps). Molecular velocity goes as high as 3 km/s. At V_p =3 km/s, depinning of the shock front is observed (2.0–3.2 ps). Jet molecules are accelerated to nearly 9 km/s before they strike the downstream. The yellow dotted-lines indicate the positions of the shock fronts.

a)Electronic mail: priyav@usc.edu

and steady shocked state are established by the time the shock wave starts interacting with the void. Upon the arrival of the shock wave at the void, RDX molecules are ejected from the upstream wall into the void, and eventually collide with the downstream wall. We have observed the focusing of the molecular jet into a narrow beam. A similar jet-focusing phenomenon was observed in rectangular-shape void collapse simulation using Lennard-Jones potential.[10] We have also observed the acceleration of the jet velocity. The maximum velocity is 3 km/s at $V_p=1$ and 9 km/s at $V_p=3$ km/s. For a planar shock front impacting a flat surface, the velocity of the ejected material is known to be $2V_p$.[11] The observed maximum jet velocity of $\sim 3V_p$ at the void is thus higher than the ejected material velocity at a planar surface, which may be due to the spherical void geometry and molecular jet focusing.[10] The beam focusing (or lensing) effect concentrates the kinetic energy into a narrow cross section to accelerate the jet and thereby may have significant effect on the ignition of energetic crystals.

Figure 1 also shows a pinning-depinning transition of the shock front. At $V_p=1$ km/s, the initial shock front is straight and pinned at the void. It bends to form a bow shape around the void. The bent shock front reaches the downstream wall before the jet molecules by bypassing the void [see Fig. 1(b)]. In contrast, the shock front profile at $V_p=3$ km/s remains straight, while crossing the void [Fig. 1(d)–1(f)]. The molecular jet catches up with the shock front and the front becomes straight [Fig. 1(f)]. After the void collapses, we also observe a ring-shape secondary shock emanates from the void location.

We have observed hotspot formation by localized vibrational modes as the void collapses. Figure 2 shows vibrational temperature distribution after the void collapses at $V_p=1$ (a) and 3 km/s (b). Here a 1.5-nm-thick slice at the center of the system is shown. In both cases, the excitation of vibrational modes is enhanced as the molecular jet flows into the void. At $V_p=1$ km/s, well-localized vibrational modes at the void location are observed [Fig. 2(a)]. On the other hand, at $V_p=3$ km/s, the molecular jet penetrates into the downstream wall, causing propagation of vibrational modes ahead of the void, thereby forming a conical-shaped hotspot [Fig. 2(b)].

To study the geometrical effect on molecular decomposition processes (i.e., chemical reactivity as the void collapses), we have carried out molecular fragment analysis near the void. Figure 3 shows a series of molecular configurations around the void. Here only these molecules that are initially within 1 nm from the void surface are shown, along with the time variation of population of chemical products at $V_p=3$ km/s. (Covalent bonds with the total bond order greater than 0.3 are regarded as connected.) The fragment analysis shows two distinct reaction regimes as the void collapses: regime I (from 2 to 2.6 ps) and II (from 2.6 to 3.9 ps). During void closure, before the molecular jet collides with the downstream wall in regime I, the NO_2 fragments rapidly emerge. After the molecular jet strikes the downstream wall in regime II, a variety of chemical products such as N_2, H_2O, and HONO are found. This result is different from the previous study[19] in shocked single crystal at 3 km/s, where NO_2 was the major chemical product. The formation of N_2 molecules is consistent with the shock loading simulation at an impact velocity $V_{imp}=10$ km/s and cookoff simulations.[15]

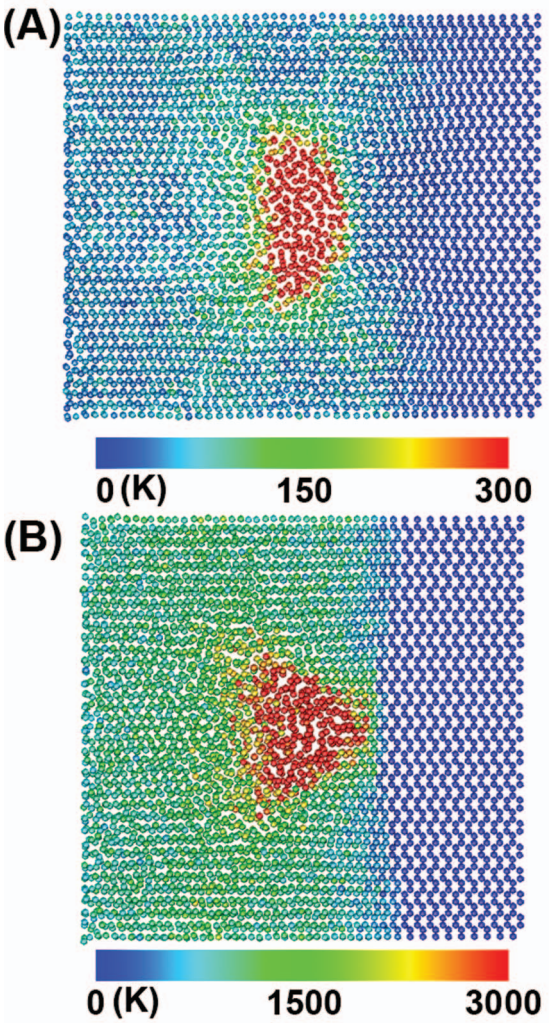

FIG. 2. (Color) Distribution of vibrational temperature around the void at 1 km/s (a) and 3 km/s (b). We observe a hemispherical hotspot (a) and a conical hotspot (b). The vibrational modes are well localized at $V_p=1$ km/s, whereas they propagate with the shock front at $V_p=3$ km/s.

In regime I, the interaction between the molecular jet and the void wall causes rapid NO_2 fragmentation. Figure 4(a) shows the distribution of NO_2 molecules viewed from the shock direction [100] at $t=2.4$ ps. The ring-shaped fragment distribution indicates that the NO_2 molecules form where the molecular jet and sidewall interact. Continuous collisions with the sidewall molecules cause energy transfer among molecules and excite vibrational modes. The NO_2 formation is due to the cleavage of an N–N bond, which is the weakest bond in an RDX molecule according to quantum-mechanical calculations in the framework of the density functional theory,[20] though experiments suggest that NO_2 is not the primary decomposition product in gas phase.[21]

In regime II, the collisions between the accelerated molecular jet and the downstream wall cause disintegration of RDX molecules. Figure 4(b) is a side view of the distribution of H_2O and N_2 molecules. The NO_2 molecules are transported to the region where the molecular jet focuses on the downstream wall and damages the crystal structure. At $t=3.9$ ps, 84% of N_2 molecules retain their initial N–N bonds while N–O and N–C bonds break in RDX molecules. On the other hand, only 2% of H_2O molecules originate from the same molecule. We have found that the large amount of ki-

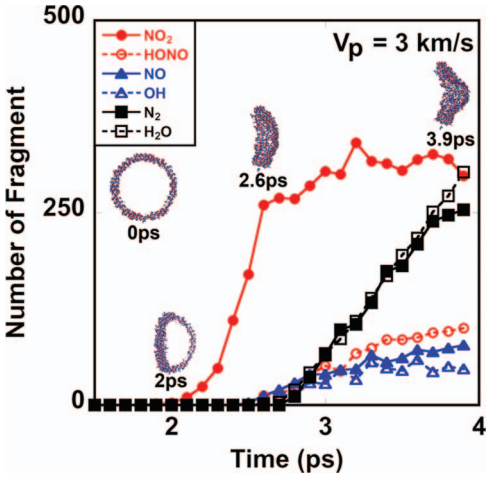

FIG. 3. (Color) Number of molecular fragments near the void surface as a function of time at V_p=3 km/s. The pictures along fragment curves show the time variation of molecular configurations within 1 nm from the void surface at t=0. For clarity, 1 nm slice of the analyzed area is shown. As the void collapses, two distinct reaction regimes are observed. From the arrival of the shock wave until the void closure (~2.6 ps), a rapid production of NO_2 is observed. Shortly after that when molecules strike the downstream wall (2.6–3.9 ps), various chemical products such as N_2, H_2O, and HONO are produced.

netic energy due to accelerated molecules causes reactions between oxygen atoms and hydrogen or oxygen atoms of neighbor molecules. Subsequently, the resulting OH radicals capture hydrogen atoms to become H_2O. Such collision-induced reactions, i.e., concerted N_2 and H_2O formation, in regime II differ from those in regime I.

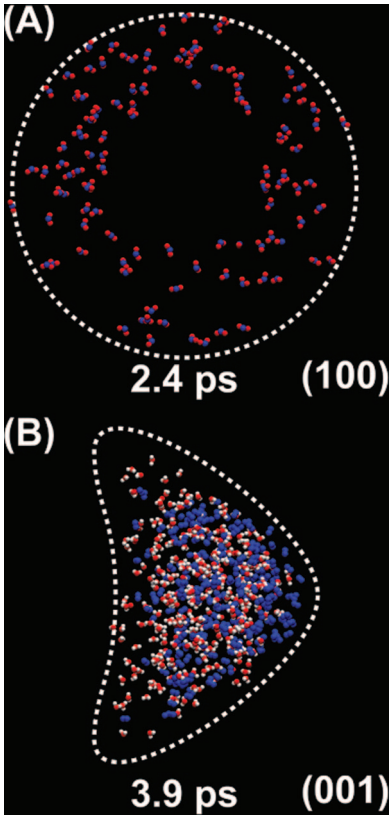

FIG. 4. (Color) Fragment distributions around the void. (a) NO_2 distribution at 2.4 ps projected on the (100) plane. (b) N_2 and H_2O distributions at 3.9 ps are projected on the (001) plane. Atoms are selected 1 nm from the void surface at t=0 and color coded as blue (nitrogen), red (oxygen), and white (hydrogen), respectively. Dotted line is added to show the envelope of molecular configurations at each time.

In summary, our million-atom reactive force field molecular dynamics simulation of shock initiation of an RDX crystal with a void shows: (1) acceleration of jet molecules through a lensing effect, (2) excitation of vibrational modes by intermolecular collisions enhanced by the free volume of the void (entropy effect), and (3) a pinning-depinning transition of the shock wave front as a function of the particle velocity and the resulting localization-delocalization transition of the vibrational energy. These factors significantly reduce the threshold for the onset of chemical reactions, thereby increasing the sensitivity of energetic material. We have found that molecules in flow are more reactive than those in compressed high-pressure state due to increased free volume and the resulting enhancement of low-frequency vibrations of NO_2 group. We have also identified two characteristic regimes in chemical product formation near the void: (1) NO_2 formation until the void closes completely and (2) subsequent production of N_2 and H_2O. Our simulation also shows void annihilation without any chemical reaction at V_p=1 km/s, implying desensitization of the energetic material.

This work was partially supported by ARO-MURI, DTRA, DOE, and NSF. Simulations were performed at DoD Major Shared Resource Centers under a Challenge award and at the University of Southern California using the 5472-processor Linux cluster at the Research Computing Facility and the 2048-processor Linux clusters at the Collaboratory for Advanced Computing and Simulations.

[1]J. C. T. Eijkel and A. van den Berg, Microfluid. Nanofluid. **1**, 249 (2005).
[2]N. K. Bourne, Shock Waves **11**, 447 (2002).
[3]K. Takayama and T. Saito, Annu. Rev. Fluid Mech. **36**, 347 (2004).
[4]M. M. Hurley, C. F. Chabalowski, G. H. Lushington, and D. Sorescu, Abstr. Pap. - Am. Chem. Soc. **220**, U284 (2000).
[5]K. L. McNesby, A. W. Miziolek, T. Nguyen, F. C. Delucia, R. R. Skaggs, and T. A. Litzinger, Combust. Flame **142**, 413 (2005).
[6]W. H. Wilson, M. P. Kramer, and R. W. Armstrong, Abstr. Pap. - Am. Chem. Soc. **221**, U608 (2001).
[7]V. Yang, T. B. Brill, and W. Z. Ren, *Solid Propellant Chemistry, Combustion, and Motor Interior Ballistics* (AIAA, Reston, VA, 2000).
[8]R. A. Yetter, F. L. Dryer, M. T. Allen, and J. L. Gatto, J. Propul. Power **11**, 683 (1995).
[9]J. P. Dear, J. E. Field, and A. J. Walton, Nature (London) **332**, 505 (1988).
[10]T. Hatano, Phys. Rev. Lett. **92**, 015503 (2004).
[11]B. L. Holian, T. C. Germann, J. B. Maillet, and C. T. White, Phys. Rev. Lett. **89**, 285501 (2002).
[12]J. W. Mintmire, D. H. Robertson, and C. T. White, Phys. Rev. B **49**, 14859 (1994).
[13]A. Tokmakoff, M. D. Fayer, and D. D. Dlott, J. Phys. Chem. **97**, 1901 (1993).
[14]A. C. T. van Duin, S. Dasgupta, F. Lorant, and W. A. Goddard, J. Phys. Chem. A **105**, 9396 (2001).
[15]A. C. T. van Duin, A. Strachan, S. Stewman, Q. S. Zhang, X. Xu, and W. A. Goddard, J. Phys. Chem. A **107**, 3803 (2003).
[16]W. J. Mortier, S. K. Ghosh, and S. Shankar, J. Am. Chem. Soc. **108**, 4315 (1986).
[17]A. K. Rappe and W. A. Goddard, J. Phys. Chem. **95**, 3358 (1991).
[18]A. Nakano, R. K. Kalia, K. Nomura, A. Sharma, P. Vashishta, F. Shimojo, A. C. T. van Duin, W. A. Goddard, R. Biswas, and D. Srivastava, Comput. Mater. Sci. **38**, 642 (2007).
[19]K. Nomura, R. K. Kalia, A. Nakano, P. Vashishta, A. C. T. van Duin, and W. A. Goddard III, Phys. Rev. Lett. **99**, 148303 (2007).
[20]D. Chakraborty, R. P. Muller, S. Dasgupta, and W. A. Goddard, J. Phys. Chem. A **104**, 2261 (2000).
[21]X. S. Zhao, E. J. Hintsa, and Y. T. Lee, J. Chem. Phys. **88**, 801 (1988).